Cement and Concrete Research 147 (2021) 106501

Contents lists available at ScienceDirect

Cement and Concrete Research

journal homepage: www.elsevier.com/locate/cemconres

Amino acids as performance-controlling additives in carbonation-activated cementitious materials

Rakibul I. Khan [a], Warda Ashraf [a,*], Jan Olek [b]

[a] Department of Civil Engineering, Center for Advanced Construction Materials (CACM), The University of Texas at Arlington, TX 76010, USA
[b] Lyles School of Civil Engineering, Purdue University, IN 47907, USA

ARTICLE INFO

Keywords:
Carbonation
Calcium silicate
Calcium carbonate
Amino acids
Wollastonite

ABSTRACT

This article presents an investigation on the application of amino acids to control the $CaCO_3$ crystallization in carbonation cured wollastonite composites. It was observed that wollastonite carbonated without any amino acid formed calcite as the primary polymorph of $CaCO_3$. In contrast, the use of amino acids as admixtures resulted in the formation of stable amorphous calcium carbonate (ACC), vaterite, and aragonite during the carbonation of wollastonite. The carbonated composites produced with amino acids were observed to have a lower critical pore size, but a higher total porosity, compared to the control batch. Additionally, the utilization of amino acids was observed to increase the flexural strength and compressive strength of the composites up to 106% and 48%, respectively, compared to the control batch. Such performance enhancement of the carbonated composites in the presence of amino acids was attributed to the reduced critical pore size and the formation of organic-inorganic hybrid phases in the matrix.

1. Introduction

Concrete or cement-based composites are responsible for up to 9% of global man-made CO_2 emissions [1]. Production of ordinary Portland cement (OPC) is also one of the most energy-intensive manufacturing processes [2]. Utilization of alternative cementitious materials instead of OPC may allow us to achieve a lower CO_2 footprint from concrete and other cement-based composites [3,4]. Carbonation-activated (or CO_2-cured) calcium silicate is one such alternative cementitious material [5–7]. The hardening process of this type of cementitious material involves the reaction of calcium silicates with CO_2 in the presence of moisture (addressed as 'carbonation or CO_2 curing') [8,9]. The carbonation reaction products of calcium silicates are $CaCO_3$ and Ca-modified silica gel (Ca/Si atomic ratio ~ 0.4), which act as the binding phases and provide strength to the hardened matrix [10,11]. This hardened matrix will be referred to as 'carbonated cement composite' for the remainder of this article. During the carbonation reaction, these composites can also store up to 18% (by wt.) of CO_2 and therefore, presents an attractive opportunity for CO_2 sequestration as well [12–14].

Previous studies have shown that the mechanical performances of these carbonated cement composites are significantly influenced by the crystalline properties of $CaCO_3$ [5,6]. In the case of calcium silicate-containing cementitious materials, the primary polymorphs of $CaCO_3$ formed during the carbonation include calcite, aragonite, vaterite, and amorphous calcium carbonate (ACC) [15–17]. Formation of these polymorphs of $CaCO_3$ ideally should follow the Ostwald's process; that is, the least stable polymorph ACC is the first to nucleate, which then crystallizes to form vaterite or aragonite (also metastable), and finally, forms calcite — the most stable polymorph [18–20]. Nevertheless, this conversion route of $CaCO_3$ polymorphs in carbonated cement composites is affected by several factors including relative humidity [21], CO_2 concentration [22], pH [23], silica content [24], and magnesium content [25]. Because of these factors, it is difficult to control the relative proportions of the different $CaCO_3$ polymorphs formed in the carbonated composites. Further, the intrinsic properties of these $CaCO_3$ polymorphs are significantly different. As an example, the stiffness of vaterite, aragonite, and calcite are 39.13 GPa, 67 GPa, and 72.83 GPa, respectively [26] (data not available for ACC). The variation in the relative proportions of different $CaCO_3$ polymorphs along with their various intrinsic characteristics often results in significant variability in the mechanical performance of carbonated cement composites. Previous studies have shown that 20 to 40% variation in the mechanical performances (i.e., strength and Young's modulus) of the carbonated

* Corresponding author.
E-mail address: warda.ashraf@uta.edu (W. Ashraf).

https://doi.org/10.1016/j.cemconres.2021.106501
Received 22 October 2020; Received in revised form 7 April 2021; Accepted 23 May 2021

composites produced in a similar carbonation setup can be observed due to the presence of different polymorphs of $CaCO_3$ [27]. Developing the ability to control the $CaCO_3$ polymorph formation and stabilization in carbonated cement composites will enable microstructure-based design optimization of this sustainable cementitious system.

While controlling the polymorphs of $CaCO_3$ in carbonated cement composites is a new concept, this approach has been widely used to produce bio-inspired materials [28]. Studies on biomineralization processes have shown that living organisms use organic matrices to control the structure and properties of the $CaCO_3$ mineral [29], specifically, to stabilize typically metastable ACC, aragonite, and vaterite polymorphs (addressed as $mCaCO_3$) [30,31]. A series of organic molecules have been identified that control the nucleation, polymorphic selection, and crystal growth of the $CaCO_3$ in biominerals [32,33]. This process of controlling the crystallization of inorganic $CaCO_3$ with organic molecules has also shown to produce 'organic-inorganic' hybrid phases with remarkable strength, toughness, and resilience [34]. Consequently, in the past several years, the selective formation of $mCaCO_3$ using organic biomimetic molecules has been extensively studied to develop materials with extraordinary characteristics [35–37]. Repetitive success has been observed using amino acids, including aspartic acid (poly) [30,38–40], serine [33], and arginine [41], to control the crystallization of $CaCO_3$. In this regard, a recent study by Kim et al. [40] investigated the effects of amino acids on the single calcite crystal. The authors [40] reported that the presence of amino acids indeed formed an organic-inorganic nanocomposite/hybrid phase with superior hardness compared to the pure calcite crystal (Fig. 1).

Inspired by these previously published findings and considering that $CaCO_3$ is the primary binder in producing carbonated cement composites, we hypothesized that amino acids can enhance the performance of these composites by altering the polymorphs of $CaCO_3$. The experimental findings presented in this article were designed to verify the above-stated hypothesis. Based on the experimental tasks, this article answered two questions:

(i) is it possible to stabilize the $mCaCO_3$ phases in carbonated cement composites by mimicking the biomineralization process?
(ii) how such formation of $mCaCO_3$ polymorphs affects the strength and microstructure of the carbonated cement composites?

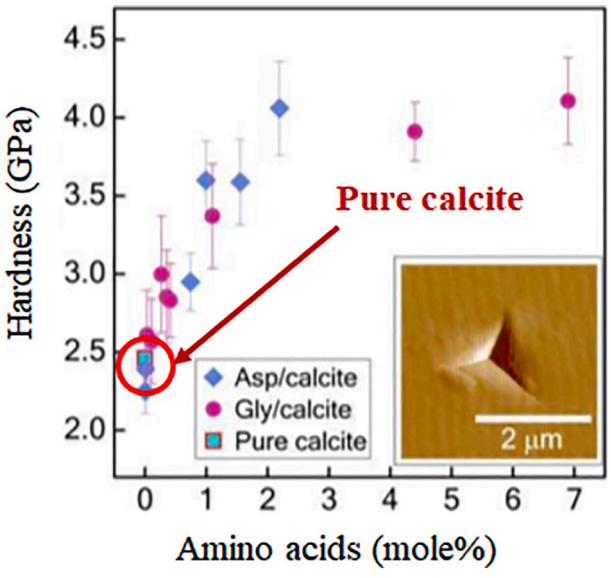

Fig. 1. Effects of amino acids on the hardness of $CaCO_3$ crystals. (Reproduced with permission from [40].)

2. Materials and methods

2.1. Raw materials

Three hydrophilic and soluble amino acids were used in this study: positively charged L-arginine (L-Arg), negatively charged L-aspartic (L-Asp) and non-polar L-serine (L-Ser). These amino acids were procured from Sigma Aldrich, USA. Ground-natural wollastonite was used as the source of calcium silicate. Wollastonite is known as a non-hydraulic calcium silicate and do not produce calcium silicate hydrate gel due to the addition of water. Therefore, it was selected as a model calcium silicate mineral to investigate carbonation behavior without significant influence from hydration reaction. This wollastonite was procured from a commercially available source (NYCO minerals, USA). The mean particle size of the ground wollastonite was 9 μm and the specific surface area was 1.6 m^2/g.

2.2. Sample preparation

Two categories of samples were prepared for carbonation in this study: (i) thin paste samples (<2 mm) without any compaction, and (ii) compacted paste cube and beam samples. The first category of samples (described in Section 2.2.1) were used to monitor the $CaCO_3$ polymorph formation and evolution over time during carbonation without the effect of CO_2 diffusion across the sample dimensions. The second category of samples (described in Section 2.2.2) were used for mechanical strength and pore size distribution analysis.

2.2.1. Carbonation of thin paste samples without compaction

Dry amino acids were first mixed with water at 0.13 M and 0.25 M concentrations. Wollastonite powder was then hand-mixed with these amino acid containing solutions for 2 min. The solution to solid (wollastonite) ratio by weight was maintained at 0.42. A control batch was prepared by mixing ground wollastonite with water without the presence of any amino acid in the same ratio. These paste-like mixtures were then spread on plastic plates and exposed to carbonation. The paste samples had around 2 mm thickness on the plate. Any possible compaction was intentionally avoided to eliminate the effects of CO_2 diffusion across the thickness of the paste sample. Carbonation was performed at 80% RH, 15% CO_2, 55 °C, and at atmospheric pressure. This experimental setup was found to be suitable for the carbonation of calcium silicates based on previously published studies [27,42]. A commercially available carbonation chamber (CO_2 incubator by VWR) was used to control these environmental parameters. Carbonated samples were collected from the chamber at intervals of 30 min, 3 h, 6 h, 24 h, 48 h, 72 h, and 145 h. After the samples were removed from the carbonation chamber, they were kept in a laboratory-sealed environment for at least 24 h before performing the characterization tests. The samples were then examined using Thermogravimetric Analysis (TGA) with or without mass spectrometer, Fourier Transformed Infrared (FTIR) and X-ray Diffraction (XRD) to monitor the extent of carbonation and the polymorph of $CaCO_3$.

2.2.2. Carbonation of paste cube and beam samples

For mechanical performance testing, paste samples were prepared with the same mix proportions as described in Section 2.2.1. In this case, mixing was performed using a rotary mixer for 2 min. The paste mixtures samples were then poured into 25 mm cube and 12.7 mm × 45 mm × 20 mm beam molds. The paste mixture had low viscosity and it was relatively easy to pour the mixtures into the beam molds. Nevertheless, all the samples were lightly tamped about 10 times with a glass rod to achieve the same level of compaction. The cube samples were exposed to CO_2 containing environment, same one as that described in Section 2.2.1, immediately after casting. The beam samples were exposed to an atmospheric pressure carbonation in a chamber with 99.9% CO_2, 55 °C, 80% RH for a duration of 300 h. A higher CO_2 concentration for beam

samples was implemented to ensure maximum possible degree of carbonation. After the initial 24 h of carbonation in the molds both, the cube and beam samples were demolded, and the carbonation process continued under the same conditions as discussed above.

2.3. Test methods

A commercially available instrument (TA instrument, TGA 55) was used for the TGA measurements. The paste samples prepared as per Section 2.2.1 were first ground using a mortar-and-pestle to obtain powder samples. Approximately 30–45 mg of this powder sample was then tested for each batch. The powdered sample was loaded into the pan and kept under isothermal conditions for 5 min. The temperature of the chamber was then raised continuously up to 980 °C with an increment of 10 °C per minute. Nitrogen gas was purged in the chamber to ensure an inert environment.

For a limited number of samples, TGA was coupled with a mass spectrometer (MS). This coupled TGA-MS system enabled the separation and identification of any volatile species coming off the sample during the heating process. In this case, TGA was performed using a Netzsch STA 449 F3 Jupiter Simultaneous Thermal Analysis (STA) instrument. All samples were measured under ultra-high purity helium gas (flow of 50 ml/min). The temperature was increased at a rate of 10 °C/min and gases were transferred to the GC/MS instrumentation via a heated (250 °C) transfer line. An Agilent Technologies 7890A GC system equipped with a non-polar capillary column (Agilent J&B HP-5 packed with [5%-phenyl-methylpolysiloxane]) coupled with a 5975 MSD spectrometer was used for the analyses of the gases released from the samples. A gas injection was triggered every minute (60 s) from the beginning of the heating cycle, and 0.25 ml of gas was sampled from the gases released by the compound and carrier gas (He).

X-ray Diffraction (XRD) patterns of the carbonated powdered samples were recorded via Bruker D-8 spectrometer using a Cu Kα radiation (40 kV, 40 mA). The diffraction patterns were obtained for the 2θ range of 5° to 60° using a step size of 0.02 (2θ) per second. For additional series of samples, 10 wt% of TiO_2 was used as the internal standard for performing Rietveld refinement. The Rietveld refinement was performed using a commercially available software (Match! Phase Analysis using Powder Diffraction). The PDF card numbers used were as follows: PDF# 96-900-5779, PDF #96-901-5391, PDF #96-901-3800, PDF #96-901-5899, and PDF #96-7250-6076 for wollastonite, calcite, aragonite, vaterite and TiO_2, respectively. However, due to the possible error in calculations, the obtained phase proportions were regarded as semi quantitative.

Scanning Electron Microscopy (SEM) images were obtained using a Zeiss-FIB SEM which was operated in high vacuum mode, using an accelerating voltage of 5 kV. Fractured surfaces of the samples were coated with gold-palladium to achieve adequate conductivity.

The Fourier-Transformed Infrared (FTIR) spectra of the ground paste sample was collected using Attenuated Total Reflection (ATR) mode with 4 cm^{-1} resolution and 16 scans for each sample. Signal to noise ratio was lower than 3:1.

The 5 × 5 × 5 mm paste cube samples were removed from the 25 mm cubes (curing condition as per Section 2.2.2) for porosity evaluation. Fig. 2 shows the location of the test samples. A slow speed diamond saw was used to remove the samples. Pore size distributions of the samples were evaluated using mercury intrusion porosimeter (MIP).

The cube and beam samples prepared as per Section 2.2.2 were used for compressive and flexural strength tests, respectively. The compression test was performed at a displacement rate of 0.02 mm per second. The flexural strengths of the carbonated paste samples were measured in 3-point bending mode using a displacement rate of 0.3 mm per second.

3. Results

3.1. Polymorph identification of metastable $CaCO_3$

FTIR spectra and XRD patterns were collected to identify the polymorphs of $CaCO_3$ formed in the carbonated wollastonite composites with and without amino acids. Fig. 3 shows the FTIR spectra of these composites after different carbonation durations. The peaks below 700 cm^{-1} wavenumbers originated from raw wollastonite. The broad absorptions between 800 cm^{-1} and 1200 cm^{-1} in the FTIR spectra of unreacted wollastonite (0 min, Fig. 3 (a)) correspond to the asymmetrical stretching vibration (ν_3) of the Si—O bond in this mineral [43]. The absorption bands of pure wollastonite at or below 800 cm^{-1} corresponds to the out-of-plane skeletal (ν_4) and in-plane skeletal (ν_2) vibrations of the Si—O bond [44,45]. During the carbonation, the gradual removal of Ca^{2+} from wollastonite increases the silicate polymerization [11], which is reflected by the shift of the ν_3 vibration of the Si—O bond to a higher wavenumber resulting from the increased bond strength [44,46].

The absorption bands for $CaCO_3$ polymorphs based on the literature are given in Table 1. The symmetric stretch (ν_1) of carbonate minerals at around 1080 cm^{-1} is often used to differentiate polymorphs of $CaCO_3$ [47]. However, this peak was overlapped by the ν_3 peak of the Si—O bond in the carbonated wollastonite composites, and hence, was not usable for $CaCO_3$ polymorph identification. The information presented in Table 1 was used to identify the $CaCO_3$ polymorphs present in carbonated wollastonite composites based on FTIR spectra.

The control batch contained ACC and/or vaterite after 30 min of carbonation, as identified by the broad peak at 1480 cm^{-1}, due to the ν_3 vibration of CO_3^{2-} (Fig. 3(a)). The control batch exhibited structural rearrangement of carbonate phases after 3 h of carbonation, as was apparent by the shift and narrowing of the ν_3 peak at 1420 cm^{-1}. The relatively sharp peak at around 1420 cm^{-1} was indicative of stable calcite formation in this system [48]. The sharp in-plane bending (ν_4) at 712 cm^{-1} and the out-of-plane bending (ν_2) at 872 cm^{-1} also confirmed the presence of only calcite polymorphs in this system (Fig. 3(a)). The ν_3 vibration of the Si—O bond at 1100 cm^{-1} and 1200 cm^{-1} indicated the formation of highly polymerized silica gel networks in this composite [8].

The ν_3 vibration of CO_3^{2-} in the L-Arginine-containing carbonated composites was around 1450 cm^{-1} (Fig. 3(b)), indicating the formation of aragonite in these systems [49]. A small peak of carbonate out-of-plane bending vibration (ν_2) at 856 cm^{-1} was observed after 72 h of carbonation, which is also the characteristic of aragonite [47]. Nevertheless, all other typical calcite peaks (712 cm^{-1} and 872 cm^{-1}) were present in the FTIR spectra of L-arginine-containing carbonated

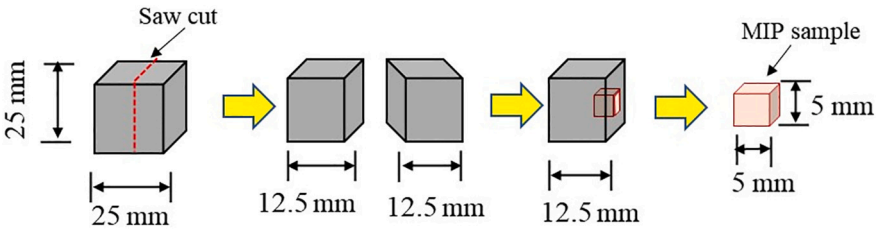

Fig. 2. Schematic showing the steps of collecting the MIP sample.

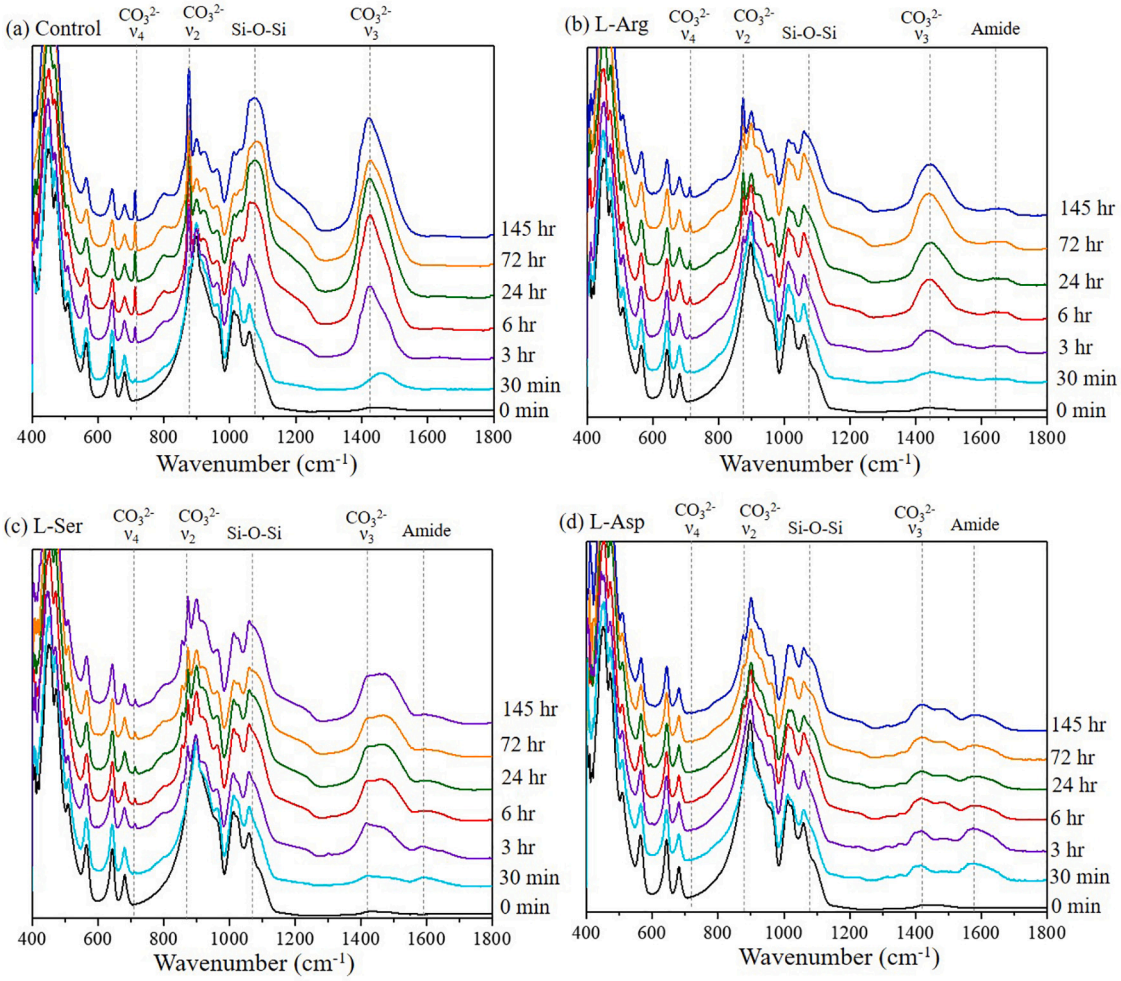

Fig. 3. FTIR spectra of carbonated wollastonite: (a) without any amino acid, (b) with 0.25 M of L-arginine, (c) with 0.25 M of L-serine, and (d) with 0.25 M of L-aspartic acid (normalized with respect to maximum peak height).

Table 1
Wavenumbers (cm^{-1}) of FTIR absorption peaks for different $CaCO_3$ polymorphs [47–50].

$CaCO_3$ polymorphs	Symmetric stretch (ν_1)	In-plane bending (ν_2)	Stretching vibration (ν_3)	Out of plane bending (ν_4)
Calcite	1080	872	1420 (relatively narrow)	712
Aragonite	1083	856	1450, 1470	700, 712
Vaterite	1087	876	1490, 1450 (broad peak)	744 (broad peak)
ACC	1067	864	1420 to 1480 (split peak)	Absent or very broad peak

composites, confirming calcite was still the primary polymorphs of $CaCO_3$ in these samples. The additional peak at around 1640 cm^{-1} as observed in Fig. 3(b) was an overlap between the OH bend present in the bound water of calcium carbonate with the amide-I vibration of amino acids [51].

The L-serine-containing carbonated composite showed similar FTIR characteristics to the L-arginine batch after 30 min of carbonation (Fig. 3 (c)). After 3 h of carbonation, the ν_3 vibration of the L-Serine batch presented a broad peak in the range of 1420 cm^{-1} to 1490 cm^{-1} representing the typical characteristics of vaterite and ACC [48]. The peak at 712 cm^{-1} was short (compared to the control) for L-serine batches, indicating the presence of only a small amount of calcite. The formation of stable aragonite in this system was identified by the ν_2 peak of carbonate ions at 856 cm^{-1} after 3 h of carbonation ((Fig. 3(c)). All the above-specified observations confirmed that L-serine-containing carbonated composites had stable ACC, vaterite, and aragonite in the matrix.

The split ν_3 peak of carbonate ions around 1420–1480 cm^{-1}, as observed in the L-aspartic acid batches (Fig. 3(d)), indicated the presence of ACC in these composites. The split ν_3 peak results from the lack of symmetry in CO_3^{2-} ions, which are the characteristic of the ACC phase [52]. The in-plane bending (ν_4) at 712 cm^{-1} was completely absent in the L-aspartic acid batches, confirming that calcite was not present in these samples. No trace of aragonite was observed in L-aspartic acid-containing composites. Therefore, ACC was the primary $CaCO_3$ polymorph formed in the L-aspartic acid-containing composites.

A comparison of the FTIR spectra of carbonated composites after 145 h of carbonation with and without amino acids (0.25 M) is given in Fig. 4. The characteristic in-plane bending (ν_4) at 712 cm^{-1} for calcite was most intense for the control batch without any amino acid. With the addition of amino acids, ν_4 at 712 cm^{-1} was reduced or disappeared, the out-of-plane bending at 872 cm^{-1} (calcite) became shorter or shifted to 856 cm^{-1} (aragonite), and the ν_3 peak at around 1420 cm^{-1} became broader (in the case of L-Arg and L-Ser) or showed split peaks (in case of L-Asp). These changes in CO_3^{2-} confirm that the addition of amino acids reduced the amounts of calcite formation and stabilized the typically

metastable $CaCO_3$ polymorphs, including ACC, vaterite, and aragonite, at room temperature in carbonated composites. Moreover, the 3D-networks of silicate species (Si^*-$(OSi)_3$) that are present in silica gel, as identified by the absorption peaks at around 1100 cm^{-1} and 1200 cm^{-1}, were most intense in the batch without any amino acid. With the addition of amino acids, these peak intensities for silica gel were reduced (Fig. 4). Thus, this study revealed that the amount of fully polymerized silica gel in carbonated cement composites can be lowered by introducing amino acids in these systems. Noteworthy, additional batches of this 145 h carbonation cured carbonated composites containing amino acids were kept in a lab environment (room temperature, 50–60% RH) for two years. The FTIR spectra of the two years old samples are given as supplementary Fig. S1. As observed from Fig. S1, after the two years of exposure, the FTIR spectra of these samples are similar to those shown in Fig. 4. Specifically, the L-Asp containing specimens still did not show any calcite peaks after two years of exposure to laboratory environment (23 °C, 50 to 60% RH). The ν_3 peaks for all the amino acid-containing batches also remained the same. These findings indicate that the presence of amino acids stabilized the formed aragonite, vaterite, and ACC for an extended period of time (at least two years), if not permanently.

XRD patterns of the wollastonite matrixes carbonated for 145 h with and without amino acids are given in Fig. 5. The XRD patterns supported the above-discussed findings of FTIR spectra. That is, calcite was the only polymorph of $CaCO_3$ present in the control batch. On the other hand, the batches containing amino acids had typical forms of $mCaCO_3$. After the control batch, the L-arginine batch had the second-highest intensity for calcite followed by the L-serine batch. The L-aspartic acid batch did not have any peak for calcite, confirming this polymorph was not present in the L-aspartic acid batches. Vaterite and aragonite were present in both the L-serine and L-arginine batches. The presence of ACC was not observed in the XRD patterns due to the relatively small amount (compared to the raw wollastonite) and the lack of crystallinity in that phase.

Rietveld refinement was performed to compare the relative proportion of the phases (Fig. 6) in the carbonated wollastonite systems. Important to note, the amorphous phase in XRD contains amorphous calcium-silica gel (carbonation reaction product), ACC, and part of unreacted wollastonite. Nevertheless, L-Asp containing batch showed the highest amount of amorphous phase present in the carbonated system, indicating the presence of ACC. The amount of unreacted wollastonite was highest in L-Ser containing batch and lowest for the control batch. This finding further confirms that the addition of amino acids reduced the carbonation extent of wollastonite. The control batch was found to contain primarily calcite form of $CaCO_3$ with relatively small

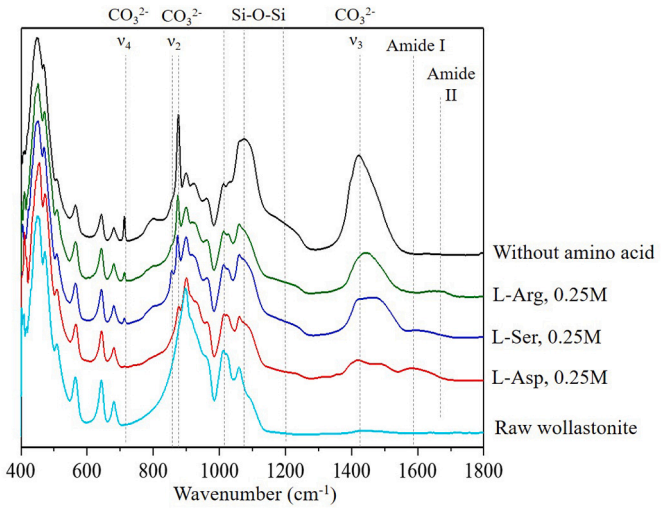

Fig. 4. A comparison of the FTIR spectra of carbonated wollastonite with and without amino acids after 145 h of carbonation.

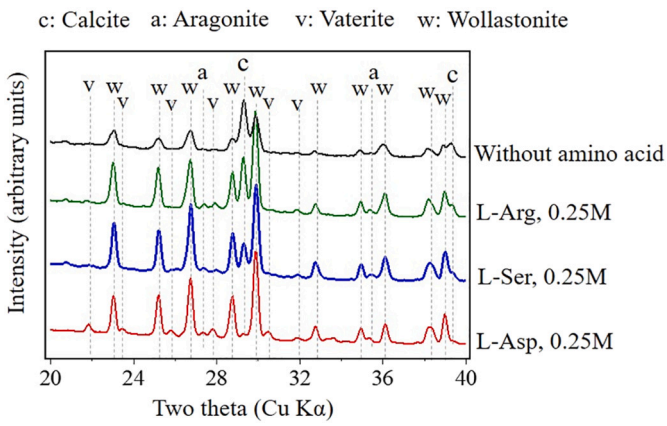

Fig. 5. X-ray Diffraction patterns showing the effects of amino acids on the polymorphs of $CaCO_3$ after 145 h of carbonation.

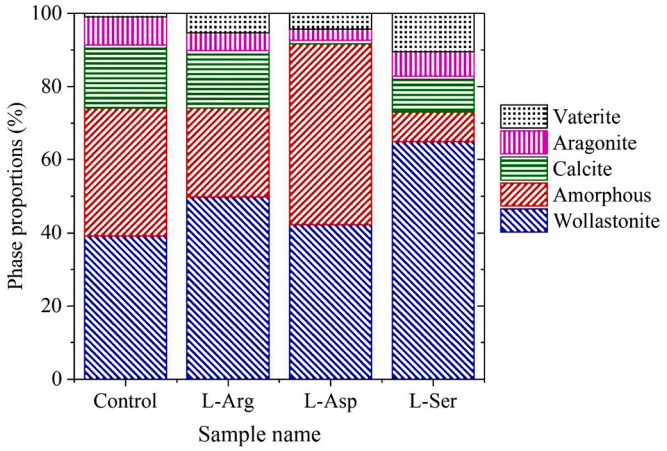

Fig. 6. Quantitative phase proportions in the 145-hour CO_2 cured composites

amounts of aragonite and vaterite. The addition of L-Arg reduced the amount of calcite and increased the amounts of aragonite and vaterite. Interesting to note, calcite was not observed to form in the L-Asp containing batch of specimens. Among the crystalline polymorphs of $CaCO_3$, vaterite was the most abundant phase in the L-Asp containing batch. L-Ser-containing batch of specimens was found to have nearly equal amounts of calcite, aragonite, and vaterite.

3.2. *Morphology of the $CaCO_3$ particles*

The SEM images were used to examine the effects of amino acids on the morphology of $CaCO_3$ particles in the scarbonated composites (Fig. 7). The SEM images were collected from carbonated composites after 300 h of carbonation. Cubic or rhombohedral crystals of calcite were prominent in the control batch (Fig. 7(a)). For this sample, the sizes of the calcite crystals were in the range of 2 to 5 μm. In the case of a carbonated composite containing 0.25 M L-Arginine, the $CaCO_3$ crystal shapes were still cubic, however, the sizes were significantly smaller (less than 1 μm, Fig. 7(b)). Thus, L-arginine mainly affected the size of the carbonates and the primary polymorph was still calcite. This matches the finding of FTIR and XRD regarding the L-arginine batches. The presence of aragonite in this system, as observed from FTIR and XRD (Figs. 3 and 5, respectively), was challenging to identify in the SEM images. This is due to the relatively small amount of this phase present in the composite. Fig. 7(c) shows the microstructure of the carbonated composite containing 0.25 M L-aspartic acid. The microstructure of this matrix was uniform throughout the section. The formation of stable ACC

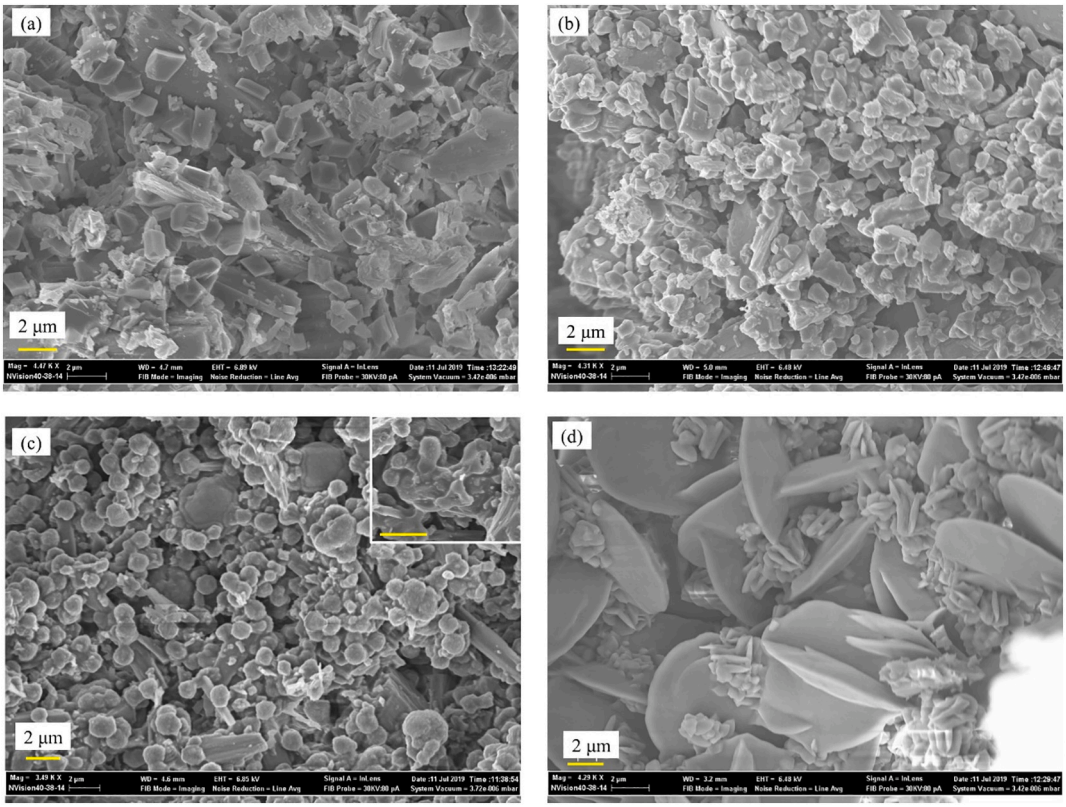

Fig. 7. SEM images (~4000×) showing microstructure of carbonated composites (a) without any amino acid, (b) with 0.25 M L-arginine, (c) with 0.25 M L-aspartic acid, and (d) with 0.25 M L-serine acid. The scale bar represents a distance of 2 µm.

was apparent from the presence of spherical $CaCO_3$ particles with around <500 nm diameter. The spherical ACC particles merged in several locations, which gave a binding capacity to the matrix (Fig. 7(c) inset). The microstructure of the batch containing 0.25 M of L-serine batch was found to have circular platy phases. Based on the FTIR and XRD data, these platy phases were identified to be vaterite crystals.

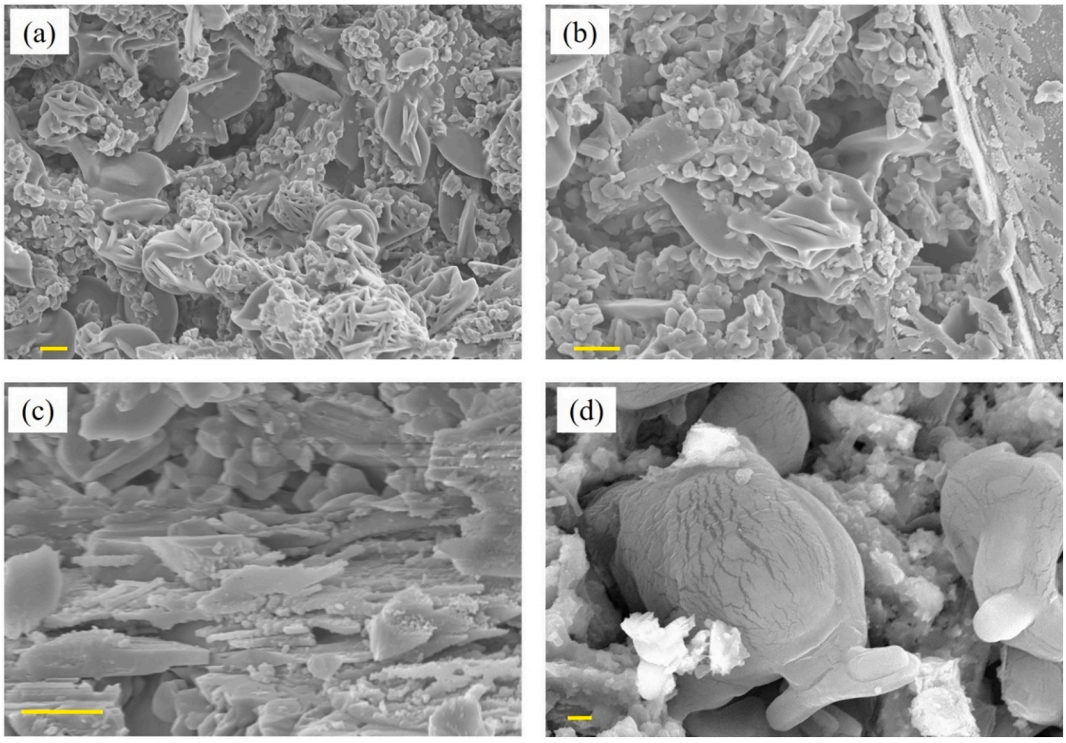

Fig. 8. SEM images showing different locations of the carbonated composite containing 0.25 M L-serine. The scale bar presents 2 µm.

Noteworthy, unlike aragonite and calcite, vaterite can show wide variability in the morphologies depending on the experimental conditions [53,54].

The microstructure of the carbonated wollastonite containing 0.25 M of L-serine aid was highly variable at different locations within the composite (Fig. 8(a) to (d)). The semi-circular plates of vaterite crystals were the most prominent phase throughout the microstructure (Fig. 8 (a)). The diameter of these plates in most of the locations was around 3 to 4 μm. The gaps between these plates were filled with smaller rhombohedral (calcite) and/or spherical (ACC) particles. The vaterite plates were also connected to form 'flower-like' shapes (Fig. 8(b)). However, in a few locations, the plates were aligned parallel, resulting in a layer-like formation (Fig. 8(c)). Such layer-like formation has long been known to be the source of high toughness of biominerals [55]. However, in some other locations, the vaterite plates were joined together to form large (~10 μm) particles (Fig. 8(d)). These particles also had parallel crack lines induced by volumetric change. These cracks likely formed due to the high vacuum pressure of the SEM chamber. The porosity around such large vaterite particles was also higher compared to other locations in the L-serine batch as well as in other batches.

3.3. Relative quantification of $mCaCO_3$ polymorphs and extent of carbonation

As discussed in the previous sections, from the FTIR, XRD, and SEM investigations, it was apparent that the presence of amino acids stabilized typical $mCaCO_3$ polymorphs including ACC, vaterite, and aragonite, in the carbonated composites. In this section, TGA with/without mass spectra (MS) was used to determine the relative proportions of $mCaCO_3$ formed in the composites and their effects on the extent of carbonation.

Fig. 9 shows the typical TGA-MS plots of carbonated composites with and without amino acids. The H_2O and CO_2 mass spectra were used to identify the origin of weight loss during the TGA measurements. As it can be observed from Fig. 9(a), the control batch showed minor weight loss due to dehydration at 100 °C; major weight loss due to the decarbonation occurred in the temperature range of 650 °C to 800 °C with the peak at 750 °C. The former weight loss was attributed to the evaporation of free water from the matrix and the later weight loss was attributed to the decomposition of $CaCO_3$ [56]. Comparing these results with those of FTIR (Fig. 3(a)) and XRD (Fig. 4), the sharp weight loss at 750 °C is considered to be the characteristic of decarbonation of calcite polymorphs of $CaCO_3$. The L-arginine-containing carbonated matrix showed an additional weight loss due to the release of H_2O at around 300 °C, which indicated the presence of chemically-bound water in this matrix (Fig. 9(b)). This weight loss was attributed to the decomposition of amino acids [57] and possible dehydration of $mCaCO_3$ [58]. Furthermore, the decomposition of $CaCO_3$ in this sample occurred at a lower peak temperature (700 °C) compared to the control batch (750 °C). Such variation in the lower decomposition temperature of $CaCO_3$ was attributed to the presence of aragonite and smaller calcite crystal sizes than those observed from FTIR (Fig. 3(b)) and SEM images (Fig. 7(b)), respectively, of this sample. Both L-serine and L-aspartic acid containing batches showed similar weight loss as that of L-arginine, due to the evaporation of free water at 100 °C and chemically-bound water at 300 °C (Fig. 9(c) and (d)). These samples also showed a gradual weight loss and a sharp weight loss due to the release of CO_2 in the temperature ranges of 200 to 650 °C and 650 °C to 800 °C, respectively, as observed from the TGA-MS plots. Comparing these TGA-MS plots with FTIR and SEM images, it is postulated that the decarbonation of vaterite (present in the L-Serine batch) and ACC (present in the L-aspartic acid batch) occurs gradually within the temperature range of 200 °C to 650 °C. Such gradual decarbonation was attributed to the poor crystalline nature of these polymorphs of $CaCO_3$. The sharp weight loss in the temperature

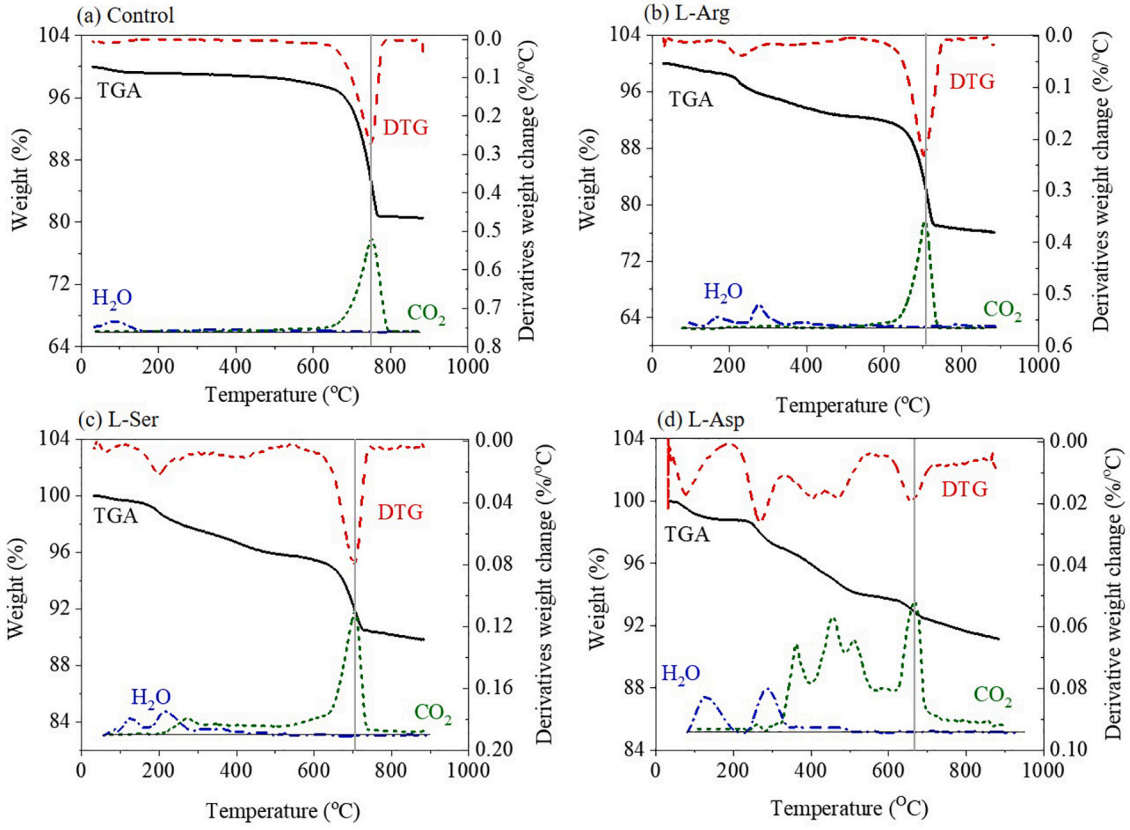

Fig. 9. TGA-MS plots showing the releases of H_2O and CO_2 gases from carbonated wollastonite matrixes: (a) control batch, (b) L-arginine, (c) L-serine and (d) L-aspartic acid containing batches.

range of 650 °C to 800 °C with the peak at 700 °C was attributed to the decarbonation of recrystallized $mCaCO_3$.

Based on these TGA-MS, FTIR, and SEM result comparisons, the gradual weight loss in the temperature range of 200 °C to 650 °C can be considered as the characteristic indicator of $mCaCO_3$ (specifically, for ACC and vaterite) formation in the carbonated matrix. Several previous studies also reported a lower decomposition temperature for vaterite and ACC [58,59]. As observed from Fig. 10(a), at higher amino acid content (0.25 M), almost all the carbonated matrixes showed this gradual weight loss in the temperature range of 200 °C to 650 °C. To compare the effectiveness of different amino acids, the relative proportions of $mCaCO_3$ compared to the total carbonates formed in the matrix was determined by the ratio of 'weight loss from 400°C to 650°C' to 'weight loss from 400°C to 800°C.' The weight loss was calculated from 400 °C (not from 200 °C) to avoid the contribution from the evaporation of chemically-bound water which occurs in the range of 200 to 350 °C. Worthy of note, this approach underestimates the amount of $mCaCO_3$ as these phases experience decarbonation in the entire range of 400 °C to 800 °C. Nevertheless, this approach provides a good semi-quantification of the $mCaCO_3$, specifically for ACC, which is difficult to quantify using traditional XRD [56]. The relative proportions of $mCaCO_3$ as determined using the above-specified approach with different carbonation duration are given in Fig. 10(c).

All the carbonated composites showed relatively high $mCaCO_3$ content at the early stage of carbonation that gradually reduced, and eventually, the relative proportion of this phase became nearly constant irrespective of the carbonation duration (Fig. 10(c)). This high amounts of $mCaCO_3$ in the initial stage was expected, since in this stage, the matrixes contain relatively small amounts of $CaCO_3$ and plenty of amino acids for stabilization. With increasing degree of carbonation, more amino acids start getting utilized which may lead to a local depletion of amino acid. Such a process can cause non-uniformity in the microstructure, resulting in the variation in the relative proportions of $mCaCO_3$ as those observed in Fig. 10(c). In case of the control batch without any amino acid, the relative proportions of $mCaCO_3$ became constant around 10 h. The stabilization of this small amount of $mCaCO_3$ in the control batch was attributed to the formation of silica gel during carbonation. Previous studies have also shown that the presence of silica can stabilize $mCaCO_3$ [24,60]. With the addition of amino acids, the relative proportions of $mCaCO_3$ were increased in the carbonated composites. Specifically, L-Aspartic acid was found to be the most effective amino acid to increase the proportion of $mCaCO_3$. As expected, for all the amino acids, 0.25 M concentration resulted in higher amounts of $mCaCO_3$ stabilization compared to 0.13 M.

The weight loss from 400 to 800 °C was further used to calculate the amount of total $CaCO_3$ formed in the carbonated samples using the stoichiometric equation ($CaCO_3 \rightarrow CaO + CO_2$). The amounts of $CaCO_3$ (% by wt of the carbonated sample) are given in Fig. 10(d). As it can be observed from this figure, the addition of amino acids resulted in lower amounts of $CaCO_3$ formation compared to the control batch after the same carbonation duration. Specifically, 0.25 M L-aspartic acid resulted in the lowest amount of $CaCO_3$ formation in the carbonated composite after 300 h of carbonation. The control batch contained approximately 1.5 times more $CaCO_3$ compared to the batches with amino acids after 300 h of carbonation. Comparing Fig. 10(c) and (d), a trend between the relative proportions of metastable $CaCO_3$ and total $CaCO_3$ after 300 h of carbonation curing is visible. Specifically, higher amounts of $mCaCO_3$ resulted in lower amounts of total $CaCO_3$ in the carbonated composites.

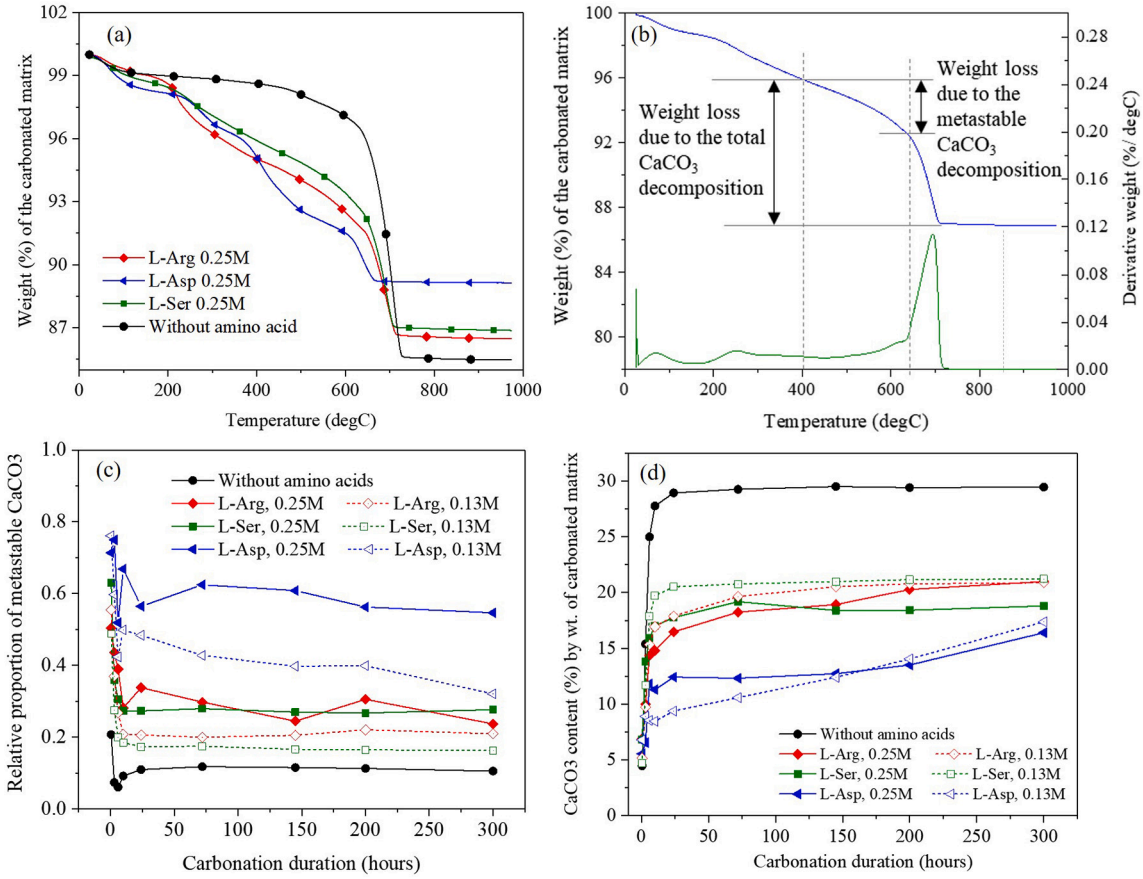

Fig. 10. (a) TGA plots of carbonated wollastonite composites with and without amino acids, (b) a sample TGA graph showing the relative weight loss due to the $mCaCO_3$ and total $CaCO_3$ in the composite, (c) relative proportions of $mCaCO_3$ with carbonation duration (hours), and (d) total $CaCO_3$ (% by weight) content in the carbonated matrices with carbonation duration.

Considering the amount of total $CaCO_3$ to be an indication of the degree of carbonation of the wollastonite, it can be suggested that a higher amount of $mCaCO_3$ formation and stabilization resulted in a lower degree of carbonation. This effect can be attributed to the following reasons:

(i) The solubility constants for calcite, aragonite, and vaterite are $10^{-8.48}$, $10^{-8.34}$, and $10^{-7.91}$, respectively [61,62]. ACC is 120 times more soluble than calcite [63]. As suggested by Morandeau and White [25], due to the high solubility of ACC, the formation of this phase makes the available solution saturated with Ca^{2+} and carbonate ions. This process, in turn, reduces the dissolution rates of calcium silicates and CO_2 in solution, and thus, also reduces the extent of carbonation [25]. A similar mechanism for reduced degrees of carbonation due to the formation of other $mCaCO_3$ composites (vaterite/ aragonite) also occurs because of their high solubility compared to calcite (stable $CaCO_3$).

(ii) The carboxyl groups ($COOH^-$) of amino acids have an unpaired electron that can bind with the Ca^{2+} ions present in wollastonite to balance the charge. This causes the amino acids to adhere to the wollastonite, resulting in a reduction of the surface area available for reaction. Such reduction of reaction sites also contributed to the observed lower degree of carbonation with the addition of amino acids. In support of this, it should be noted that L-aspartic acid, containing two negatively charged carboxyl groups ($COOH^-$), showed the lowest $CaCO_3$ formation compared to the other two amino acids, which contain one carboxyl site.

(iii) The densities of $CaCO_3$ polymorphs are; vaterite: 2.66 g/cm^3, aragonite: 2.93 g/cm^3, calcite: 2.71 g/cm^3, ACC: 1.62– 2.59 g/cm^3 depending on the H_2O content [64]. Because of such difference in density, the formation of the same amount (by weight) of vaterite and ACC, as opposed to calcite or aragonite, is understood to alter the pore size distribution of the carbonated composites [24]. As a result, the diffusivity of CO_2 in the carbonated composites can be affected if ACC or vaterite are stabilized as opposed to calcite or aragonite. A possible lower CO_2 diffusivity within the matrix, caused by different polymorphs of $CaCO_3$, will eventually lead to a lower degree of carbonation.

3.4. Effects of metastable $CaCO_3$ on pore size distributions

The pore size distributions of the carbonated composites, as determined using the Mercury Intrusion Porosimeter (MIP), are given in Fig. 11. The total pore volume in the range of 0.1 to 5 μm was higher in the amino acid containing batches than in the control batch. However, the addition of amino acids was found to reduce the critical pore size (size of the pore with maximum volume) of the matrix. The critical pore diameters of the control, L-aspartic acid, L-serine, and L-arginine batches were 1.33 μm, 1.07 μm, 0.86 μm, and 1.07 μm, respectively. The median pore sizes (i.e. sizes for which 50% of the pores were smaller and 50% were larger) of the control, L-aspartic acid, L-serine, and L-arginine batches were 0.78 μm, 1.4 μm, 0.74 μm, and 1.0 μm, respectively. Thus, the addition of amino acids resulted in a refinement of pore sizes in the carbonated composites (based on the critical pore diameter), even though the total porosity was increased. The reduction of pore size distribution was most apparent in the case of the L-Serine containing carbonated composites.

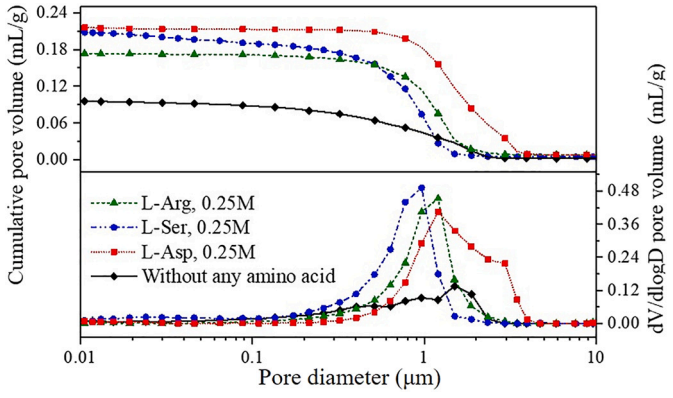

Fig. 11. Effects of amino acids on the pore size distribution of the carbonated composites.

3.5. Effects of metastable $CaCO_3$ on compressive and flexural strengths

The effects of the amino acids on the compressive and flexural strengths of the carbonated composites are presented in Fig. 12(a) and (b), respectively. As observed from these figures, both flexural and compressive strengths of the carbonated wollastonite showed increasing trends with the increasing amino acids contents. The flexural strengths of the beam were increased by 33% to 47% due to the addition of a 0.13 M of amino acids. The corresponding increases of compressive strengths due to the same dosage of amino acid solution were in the range of 2% to 33%. The addition of 0.25 M amino acid solution increases the compressive and flexural strengths of the composites by 33% to 43% and 56% to 106%, respectively. The addition of 0.25 M L-serine was found to result in maximum strengths of the composites, i.e., 48% and 106% increases of the compressive and flexural strengths, respectively, compared to the control batch. Noteworthy, the L-aspartic acid containing batch showed more consistent compressive and flexural strengths with lower standard deviation which was attributed to the uniform spherical ACC formation in the matrix.

4. Discussion

As observed in the Results section, all the carbonated composite specimens prepared with amino acids were observed to form various $mCaCO_3$ phases, including vaterite, aragonite, and ACC. Based on the concepts of biomineralization, the interaction between amino acids and calcium carbonate crystals inhibits the transition from a $mCaCO_3$ to a stable polymorph (calcite). Thus, the Ostwald step sequence is stopped at one of its intermediate stages through the inhibition or stabilization of a particular metastable polymorphic phase [31,33,65]. However, the effectiveness of the amino acids with respect to these processes was different, and it depended on their molecular characteristics. Specifically, L-aspartic acid was most effective in stabilizing the ACC polymorph of $CaCO_3$, followed by L-serine and finally L-arginine (Fig. 10(c)). It should be noted that L-Aspartic acid is negatively charged, L-arginine is positively charged, and L-serine is an uncharged amino acid. The higher efficiency of L-aspartic acid to inhibit the dissolution of ACC particles was presumably due to the negative charge of this amino acid. The negatively charged carboxyl surface sites of L-aspartic acid binds with Ca^{2+} sites of $CaCO_3$ by sharing an electron. Such a bond then inhibits further dissolution of ACC particles and the formation of stable polymorphs of $CaCO_3$ (second mechanism as discussed above) [31]. In the case of the L-serine specimens, only a partial inhibition of ACC and vaterite particle dissolution was observed in this study. The formation of calcite and vaterite in the presence of L-serine has also been reported in other biomimetic studies [66]. In the case of L-arginine, the positively charged side chain can form a stable complex with HCO_3^- [66]. This stable complex eventually leads to the formation of relatively smaller calcite and aragonite crystals, as observed with SEM and TGA (Figs. 7 and 3). In addition to the above-discussed mechanisms, amino acids can form hydrogen bonds due to the presence of amine groups, which also inhibit the dissolution of $mCaCO_3$ [33,67].

The addition of amino acids (and thus the formation of $mCaCO_3$) resulted in higher strengths of the carbonated composites (Fig. 12), even though it increased the total porosity and decreased the degree of carbonation. We propose two hypotheses for such an increase in

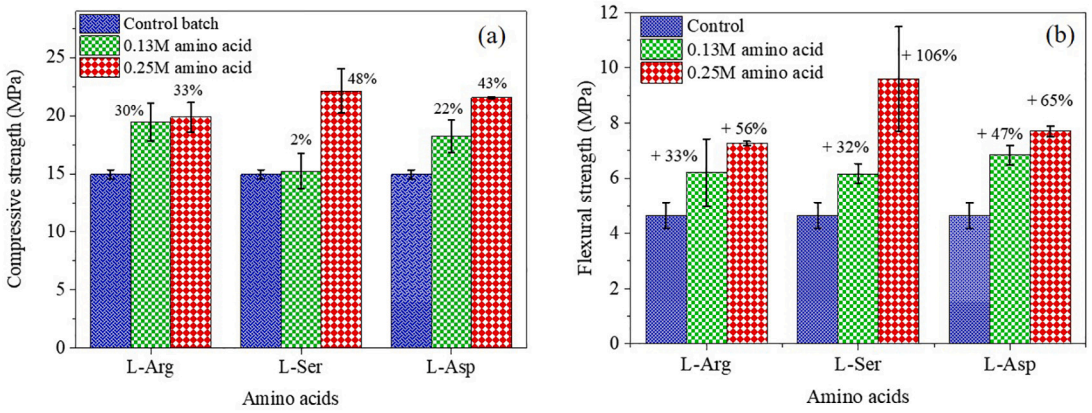

Fig. 12. Effects of amino acids on the (a) compressive strengths and (b) flexural strengths of the carbonated composites after 300 h of carbonation. Error bars represent one standard deviation.

strength. First, during the stabilization process, the organic amino acids are adsorbed on the surface of these $CaCO_3$ polymorphs, which can lead to the formation of organic-inorganic hybrids/ nanocomposites (Fig. 13). It is well known that such hybrid composites possess remarkable mechanical performance [68]. Specifically, Kim et al. [40] showed that the presence of amino acids can increase the hardness of $CaCO_3$ crystals by forming organic-inorganic nanocomposite phases. As a consequence, the enhanced mechanical strengths, as observed in this study, can be attributed to such alternation of $CaCO_3$ intrinsic properties due to the presence of amino acids. Second, in addition to the intrinsic properties of $CaCO_3$ polymorphs, the reduction of critical pore size of the carbonated matrixes due to the addition of amino acids may have also enhanced the strengths of these matrixes.

5. Conclusions

Following is the list of major observations from this study.

(1) The addition of amino acids resulted in the stabilization of typical $mCaCO_3$, namely ACC, vaterite, and aragonite, in carbonated wollastonite composites.
(2) L-Aspartic acid was most effective in stabilizing the ACC in the carbonated composites. L-Serine resulted in the stabilization of both ACC and vaterite. The effectiveness of L-arginine was more prominent in reducing the $CaCO_3$ carbonate crystal size, but not in altering the polymorphs.
(3) The formation and stabilization of $mCaCO_3$ resulted in a lower degree of carbonation of wollastonite under similar experimental conditions. Such a reduced degree of carbonation due to the addition of amino acids was attributed to their higher solubility, the adherence of amino acids to the surface of the wollastonite, and the different densities of the $mCaCO_3$ polymorphs.
(4) The total porosity of the carbonated composite was increased due to the addition of amino acids. However, amino acids decreased the critical pore diameter compared to the control batch.
(5) The carbonated composites containing amino acids showed up to 48% and 106% increase in compressive and flexural strengths, respectively, compared to the control batch.

In summary, this study provided experimental evidence that amino acids can be a potential chemical admixture to enhance the mechanical performance of carbonated calcium silicate composites. Nevertheless, additional studies are required to understand the mechanism of performance enhancement of these composites in the presence of amino acids. Such an understanding will allow us to develop non-natural, affordable, and sustainable amino acid-mimics to achieve similar

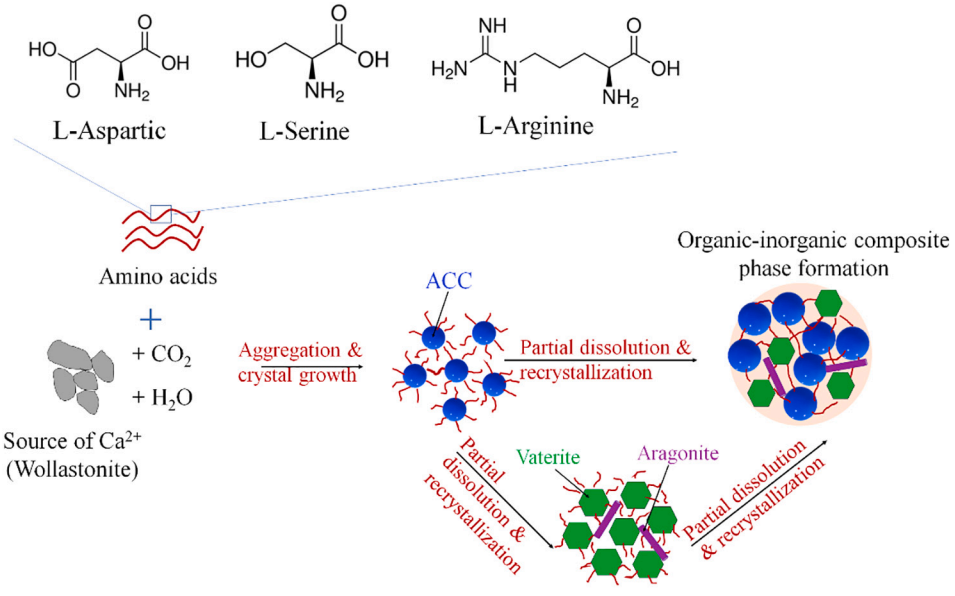

Fig. 13. Proposed mechanism of in-situ nanocomposite formation in carbonated wollastonite composites.

benefits in industrial scale production of carbonated cement composites.

Supplementary data to this article can be found online at https://doi.org/10.1016/j.cemconres.2021.106501.

CRediT authorship contribution statement

Rakibul I. Khan: Data curation, Formal analysis, Investigation, Writing – review & editing. **Warda Ashraf:** Conceptualization, Formal analysis, Writing – original draft, Investigation, Funding acquisition, Supervision, Writing – review & editing. **Jan Olek:** Writing – review & editing.

Declaration of competing interest

The authors declare that no conflict of interest is involved in this paper and the authors are responsible for the content and writing.

Acknowledgements

This work was conducted with partial funding support from the US National Science Foundation (NSF # ECI - 2028462) and the faculty start-up grant for Dr. Warda Ashraf at the University of Texas at Arlington. All opinions, findings, and conclusions or recommendations expressed in this material are those of the authors and do not necessarily reflect the views of the NSF. The TGA-MS measurements were collected using the IMSERC facilities at Northwestern University, which has received support from the Soft and Hybrid Nanotechnology Experimental (SHyNE) Resource (NSF ECCS-1542205), the State of Illinois, and the International Institute for Nanotechnology (IIN).

References

[1] J. Olivier, J. Peters, Trends in Global CO_2 and Total Greenhouse Gas Emissions 2018 Report 53, PBL Netherlands Environ. Assess. Agency, 2018.
[2] EIA, The Cement Industry Is the Most Energy Intensive of All Manufacturing Industries, 2013.
[3] C. Shi, B. Qu, J.L. Provis, Recent progress in low-carbon binders, Cem. Concr. Res. 122 (2019) 227–250, https://doi.org/10.1016/j.cemconres.2019.05.009.
[4] M.C.G. Juenger, F. Winnefeld, J.L. Provis, J.H. Ideker, Advances in alternative cementitious binders, Cem. Concr. Res. 41 (2011) 1232–1243, https://doi.org/10.1016/j.cemconres.2010.11.012.
[5] W. Ashraf, J. Olek, Carbonation activated binders from pure calcium silicates: reaction kinetics and performance controlling factors, Cem. Concr. Compos. 93 (2018) 85–98.
[6] P. De Silva, L. Bucea, D.R. Moorehead, V. Sirivivatnanon, Carbonate binders: reaction kinetics, strength and microstructure, Cem. Concr. Compos. 28 (2006) 613–620, https://doi.org/10.1016/j.cemconcomp.2006.03.004.
[7] W. Ashraf, J. Olek, J. Jain, Microscopic features of non-hydraulic calcium silicate cement paste and mortar, Cem. Concr. Res. 100 (2017) 361–372, https://doi.org/10.1016/j.cemconres.2017.07.001.
[8] W. Ashraf, J. Olek, Carbonation behavior of hydraulic and non-hydraulic calcium silicates: potential of utilizing low-lime calcium silicates in cement-based materials, J. Mater. Sci. (2016), https://doi.org/10.1007/s10853-016-9909-4.
[9] J.M. Bukowski, R.L. Berger, Reactivity and strength development of CO_2 activated non-hydraulic calcium silicates, Cem. Concr. Res. 9 (1979) 57–68.
[10] W. Ashraf, J. Olek, S. Sahu, Phase evolution and strength development during carbonation of low-lime calcium silicate cement (CSC), Constr. Build. Mater. 210 (2019) 473–482, https://doi.org/10.1016/j.conbuildmat.2019.03.038.
[11] W. Ashraf, J. Olek, Elucidating the accelerated carbonation products of calcium silicates using multi-technique approach, J. CO_2 Util. 23 (2018) 61–74, https://doi.org/10.1016/j.jcou.2017.11.003.
[12] Y. Shao, M.S. Mirza, X. Wu, CO_2 sequestration using calcium-silicate concrete, Can. J. Civ. Eng. 33 (2006) 776–784, https://doi.org/10.1139/l05-105.
[13] I. Galan, C. Andrade, P. Mora, M.A. Sanjuan, Sequestration of CO_2 by concrete carbonation, Environ. Sci. Technol. 44 (8) (2010) 3181–3186, https://doi.org/10.1021/es903581d.
[14] W. Ashraf, J. Olek, V. Atakan, Carbonation reaction kinetics, CO_2 sequestration capacity, and microstructure of hydraulic and non-hydraulic cementitious binders, in: Sustain. Constr. Mater. Technol, 2016.
[15] S. Goto, K. Suenaga, T. Kado, Calcium silicate carbonation products, J. Am. Ceram. Soc. 78 (1995) 2867–2872.
[16] G.W. Groves, A. Brough, I.G. Richardson, C.M. Dobson, Progressive changes in the structure of hardened C3S cement pastes due to carbonation, J. Am. Ceram. Soc. 74 (1991) 2891–2896, https://doi.org/10.1111/j.1151-2916.1991.tb06859.x.
[17] O. Shtepenko, C. Hills, A. Brough, M. Thomas, The effect of carbon dioxide on β-dicalcium silicate and Portland cement, Chem. Eng. J. 118 (2006) 107–118, https://doi.org/10.1016/j.cej.2006.02.005.
[18] S.A. Bernal, J.L. Provis, B. Walkley, R. San Nicolas, J.D. Gehman, D.G. Brice, A. R. Kilcullen, P. Duxson, J.S.J. Van Deventer, Gel nanostructure in alkali-activated binders based on slag and fly ash, and effects of accelerated carbonation, Cem. Concr. Res. 53 (2013) 127–144, https://doi.org/10.1016/j.cemconres.2013.06.007.
[19] S.A. Bernal, J.L. Provis, D.G. Brice, A. Kilcullen, P. Duxson, J.S.J. Van Deventer, Accelerated carbonation testing of alkali-activated binders significantly underestimates service life: the role of pore solution chemistry, Cem. Concr. Res. 42 (2012) 1317–1326, https://doi.org/10.1016/j.cemconres.2012.07.002.
[20] S.A. Bernal, R. San Nicolas, R.J. Myers, R. Mejía De Gutiérrez, F. Puertas, J.S.J. Van Deventer, J.L. Provis, MgO content of slag controls phase evolution and structural changes induced by accelerated carbonation in alkali-activated binders, Cem. Concr. Res. 57 (2014) 33–43, https://doi.org/10.1016/j.cemconres.2013.12.003.
[21] P. López-Arce, L.S. Gómez-Villalba, S. Martínez-Ramírez, M. Álvarez de Buergo, R. Fort, Influence of relative humidity on the carbonation of calcium hydroxide nanoparticles and the formation of calcium carbonate polymorphs, Powder Technol. 205 (2011) 263–269, https://doi.org/10.1016/j.powtec.2010.09.026.
[22] S. Goñi, M.T. Gaztañaga, A. Guerrero, Role of cement type on carbonation attack, J. Mater. Res. 17 (2002) 1834–1842, https://doi.org/10.1557/JMR.2002.0271.
[23] D. Gebauer, A. Völkel, H. Cölfen, Stable prenucleation calcium carbonate clusters, Science (80-.) 322 (2008) 1819–1822, https://doi.org/10.1126/science.1164271.
[24] W. Ashraf, J. Olek, Elucidating the carbonation products of calcium silicates using NMR, XRD, and vapor sorption isotherms, J. CO_2 Util. 23 (2018) 61–74, https://doi.org/10.1016/j.jcou.2017.11.003.
[25] A.E. Morandeau, Claire E. White, Role of magnesium-stabilized amorphous calcium carbonate in mitigating the extent of carbonation in alkali-activated slag, Chem. Mater. 27 (19) (2015) 6625–6634.
[26] N.K. Dhami, A. Mukherjee, M.S. Reddy, Micrographical, minerological and nano-mechanical characterisation of microbial carbonates from urease and carbonic anhydrase producing bacteria, Ecol. Eng. 94 (2016) 443–454, https://doi.org/10.1016/j.ecoleng.2016.06.013.
[27] W. Ashraf, J. Olek, Carbonation activated binders from pure calcium silicates: reaction kinetics and performance controlling factors, Cem. Concr. Compos. 93 (2018) 85–98, https://doi.org/10.1016/j.cemconcomp.2018.07.004.
[28] N.A.J.M. Sommerdijk, G. De With, Biomimetic $CaCO_3$ mineralization using designer molecules and interfaces, Chem. Rev. 108 (11) (2008) 4499–4550.
[29] L. Ma, J. Zhu, M. Cui, L. Huang, Y. Su, Biomimetic synthesis of novel calcium carbonate heterogeneous dendrites, New J. Chem. 39 (2015) 5309–5315, https://doi.org/10.1039/c5nj00219b.
[30] K. Maruyama, T. Yoshino, H. Kagi, Synthesizing a composite material of amorphous calcium carbonate and aspartic acid, Mater. Lett. 65 (2011) 179–181, https://doi.org/10.1016/j.matlet.2010.09.039.
[31] Z. Zou, L. Bertinetti, Y. Politi, P. Fratzl, W.J.E.M. Habraken, Control of polymorph selection in amorphous calcium carbonate crystallization by poly(aspartic acid): two different mechanisms, Small. 13 (2017) 1–11, https://doi.org/10.1002/smll.201603100.
[32] H. Tong, W. Ma, L. Wang, P. Wan, J. Hu, L. Cao, Control over the crystal phase, shape, size and aggregation of calcium carbonate via a L-aspartic acid inducing process, Biomaterials. 25 (2004) 3923–3929, https://doi.org/10.1016/j.biomaterials.2003.10.038.
[33] L. Štajner, J. Kontrec, B. Njegić Džakula, N. Maltar-Strmečki, M. Plodinec, D. M. Lyons, D. Kralj, The effect of different amino acids on spontaneous precipitation of calcium carbonate polymorphs, J. Cryst. Growth 486 (2018) 71–81, https://doi.org/10.1016/j.jcrysgro.2018.01.023.
[34] P. Stempfle, O. Pantale, R.K. Njiwa, M. Rousseau, E. Lopez, X. Bourrat, Friction-induced sheet nacre fracture: effects of nano-shocks on cracks location, Int. J. Nanotechnol. 4 (2007) 712–729, https://doi.org/10.1504/ijnt.2007.015466.
[35] A. Kotachi, T. Miura, H. Imai, Polymorph control of calcium carbonate films in a poly(acrylic acid)-chitosan system, Cryst. Growth Des. 6 (7) (2006) 1636–1641, https://doi.org/10.1021/cg050528l.
[36] W. Jiang, M.S. Pacella, D. Athanasiadou, V. Nelea, H. Vali, R.M. Hazen, J.J. Gray, M.D. Mckee, Chiral acidic amino acids induce chiral hierarchical structure in calcium carbonate, Nat. Commun. 8 (15066) (2017) 1–13, https://doi.org/10.1038/ncomms15066.
[37] W. Jiang, M.S. Pacella, H. Vali, J.J. Gray, M.D. Mckee, Chiral switching in biomineral suprastructures induced by homochiral L-amino acid, Sci. Adv. 4 (2018) 1–12, https://doi.org/10.1126/sciadv.aas9819.
[38] C.A. Orme, A. Noy, A. Wierzbicki, M.T. McBride, M. Grantham, H.H. Tengs, P. M. Dove, J.J. DeYoreo, Formation of chiral morphologies through selective binding of amino acids to calcite surface steps, Nature 411 (2001) 775–779, https://doi.org/10.1038/35081034.
[39] H.H. Teng, P.M. Dove, C.A. Orme, J.J. de Yoreo, Thermodynamics of calcite growth: baseline for understanding biomineral formation, Science (80-.) 282 (1998) 724–727, https://doi.org/10.1126/science.282.5389.724.
[40] Y.Y. Kim, J.D. Carloni, B. Demarchi, D. Sparks, D.G. Reid, M.E. Kunitake, C. C. Tang, M.J. Duer, C.L. Freeman, B. Pokroy, K. Penkman, J.H. Harding, L. A. Estroff, S.P. Baker, F.C. Meldrum, Tuning hardness in calcite by incorporation of amino acids, Nat. Mater. 15 (2016) 903–910, https://doi.org/10.1038/nmat4631.
[41] L. Qiao, Q. Feng, Z. Li, S. Lu, Alternate deposition of oriented calcite and amino acid layer on calcite substrates, J. Phys. Chem. B 112 (43) (2008) 13635–13640, https://doi.org/10.1021/jp8028775.

[42] W. Ashraf, J. Olek, V. Atakan, Carbonation reaction kinetics, CO_2 sequestration capacity, and microstructure of hydraulic and non-hydraulic cementitious binders, in: Sustain. Constr. Mater. Technol, 2016.
[43] I.F. Sáez Del Bosque, S. Martínez-Ramírez, M.T. Blanco-Varela, FTIR study of the effect of temperature and nanosilica on the nano structure of C-S-H gel formed by hydrating tricalcium silicate, Constr. Build. Mater. 52 (2014) 314–323, https://doi.org/10.1016/j.conbuildmat.2013.10.056.
[44] Y. Okada, T. Masuda, M. Takada, L. Xu, T. Mitsuda, Silicate anion structure and dehydration processes of okenite, J. Ceram. Soc. Jpn. 102 (1190) (1994) 919–924. Released August 06, 2010, Online ISSN 1882-1022, Print ISSN 0914-5400, https://doi.org/10.2109/jcersj.102.919.
[45] M. Yousuf, A. Mollah, J.R. Pargat, D.L. Cocke, An infrared spectroscopic examination of cement-based solidification/stabilization systems — Portland types V and IP with zinc, J. Environ. Sci. Heal. Pt A Environ. Sci. Eng. Toxicol. 27 (1992) 1503–1519, https://doi.org/10.1080/10934529209375809.
[46] P. Yu, R.J. Kirkpatrick, B. Poe, P.F. McMillan, X. Cong, Structure of calcium silicate hydrate (C-S-H): near-, mid-, and far-infrared spectroscopy, J. Am. Ceram. Soc. 82 (1999) 742–748, https://doi.org/10.1111/j.1151-2916.1999.tb01826.x.
[47] D. Chakrabarty, S. Mahapatra, Aragonite crystals with unconventional morphologies, J. Mater. Chem. 9 (1999) 2953–2957, https://doi.org/10.1039/a905407c.
[48] M. Sato, S. Matsuda, Structure of vaterite and infrared spectra, Zeitsch. Krist. New Cryst. Struct. 129 (1969) 405–410, https://doi.org/10.1524/zkri.1969.129.5-6.405.
[49] C.E. Weir, E.R. Lippincott, Infrared studies of aragonite, calcite, and vaterite type structures in the borates, carbonates, and nitrates, J. Res. Natl. Bur. Stand. Sect. A Phys. Chem. 65A (2012) 173–180, https://doi.org/10.6028/jres.065a.021.
[50] Flemming A. Andersen, Ljerka Brecevic, Infrared spectra of amorphous and crystalline calcium carbonate, Acta Chem. Scand. 45 (10) (1991) 1018–1024.
[51] W. Gallagher, FTIR analysis of protein structure, Nature. 18 (1958) 662–666.
[52] L. Addadi, S. Raz, S. Weiner, Taking advantage of disorder: amorphous calcium carbonate and its roles in biomineralization, Adv. Mater. 15 (2003) 959–970, https://doi.org/10.1002/adma.200300381.
[53] R.J. Qi, Y.J. Zhu, Microwave-assisted synthesis of calcium carbonate (vaterite) of various morphologies in water–ethylene glycol mixed solvents, J. Phys. Chem. B 110 (16) (2006) 8302–8306, https://doi.org/10.1021/jp060939s.
[54] B.G. Mao, D.Q. Chu, A.X. Wang, L.M. Wang, H.M. Sun, Z.Y. Zhang, X.Z. Yang, Fabrication of flowerlike vaterite calcium carbonate crystal aggregates by self-assembly in water/ethanol mixtures, Eur. J. Inorg. Chem. (2013) 5958–5963, https://doi.org/10.1002/ejic.201300892.
[55] E. Macías-sánchez, M.G. Willinger, C.M. Pina, A.G. Checa, Transformation of ACC into aragonite and the origin of the nanogranular structure of nacre, Sci. Rep. 7 (2017) 1–11, https://doi.org/10.1038/s41598-017-12673-0.
[56] W. Ashraf, J. Olek, Elucidating the accelerated carbonation products of calcium silicates using multi-technique approach, J. CO_2 Util. 23 (2018) 61–74, https://doi.org/10.1016/j.jcou.2017.11.003.
[57] I.M. Weiss, C. Muth, R. Drumm, H.O.K. Kirchner, Thermal decomposition of the amino acids glycine, cysteine, aspartic acid, asparagine, glutamic acid, glutamine, arginine and histidine, BMC Biophys. 11 (2018) 1–15.
[58] J. Ihli, W.C. Wong, E.H. Noel, Y.-Y. Kim, A.N. Kulak, H.K. Christenson, M.J. Duer, F.C. Meldrum, Dehydration and crystallization of amorphous calcium carbonate in solution and in air, Nat. Commun. 5 (2014) 3169, https://doi.org/10.1038/ncomms4169.
[59] B.C. Chakoumakos, B.M. Pracheil, R.P. Koenigs, R.M. Bruch, M. Feygenson, Empirically testing vaterite structural models using neutron diffraction and thermal analysis, Sci. Rep. 6 (2016) 1–9, https://doi.org/10.1038/srep36799.
[60] M. Kellermeier, E. Melero-garcı, F. Glaab, R. Klein, M. Drechsler, R. Rachel, J. M. Garcı, W. Kunz, Stabilization of amorphous calcium carbonate in inorganic silica-rich environments, J. Am. Chem. Soc. 132 (50) (2010) 17859–17866, https://doi.org/10.1021/ja106959p.
[61] L.N. Plummer, E. Busenberg, The solubilities of calcite, aragonite and vaterite in CO_2-H_2O solutions between 0 and 90 °C, and an evaluation of the aqueous model for the system $CaCO_3$-CO_2-H_2O, Geochim. Cosmochim. Acta 46 (1982) 1011–1040, https://doi.org/10.1016/0016-7037(82)90056-4.
[62] D. Ren, Q. Feng, X. Bourrat, Effects of additives and templates on calcium carbonate mineralization in vitro, Micron. 42 (2011) 228–245, https://doi.org/10.1016/j.micron.2010.09.005.
[63] O.E. Meiron, E. Bar-David, E.D. Aflalo, A. Shechter, D. Stepensky, A. Berman, A. Sagi, Solubility and bioavailability of stabilized amorphous calcium carbonate, J. Bone Miner. Res. 26 (2011) 364–372, https://doi.org/10.1002/jbmr.196.
[64] M. Saharay, A.O. Yazaydin, R.J. Kirkpatrick, Dehydration-induced amorphous phases of calcium carbonate, J. Phys. Chem. B 117 (12) (2013) 3328–3336, https://doi.org/10.1021/jp308353t.
[65] A. Rodriguez-navarro, C. Jimenez-lopez, A. Checa, J.M.G. Ruiz, Nanocrystalline structures in calcium carbonate biominerals, J. Nanophoton. (2008), https://doi.org/10.1117/1.3062826.
[66] Y. Guo, F. Wang, J. Zhang, L. Yang, X. Shi, Q. Fang, X. Ma, Biomimetic synthesis of calcium carbonate with different morphologies under the direction of different amino acids, Res. Chem. Intermed. 39 (2013) 2407–2415, https://doi.org/10.1007/s11164-012-0767-7.
[67] R. Innocenti Malini, A.R. Finney, S.A. Hall, C.L. Freeman, J.H. Harding, The water-amorphous calcium carbonate interface and its interactions with amino acids, Cryst. Growth Des. 17 (11) (2017) 5811–5822, https://doi.org/10.1021/acs.cgd.7b00874.
[68] B. Cantaert, D. Kuo, S. Matsumura, T. Nishimura, T. Sakamoto, T. Kato, Use of amorphous calcium carbonate for the design of new materials, Chempluschem. 82 (2017) 107–120, https://doi.org/10.1002/cplu.201600457.